IOP Publishing Journal of Physics B: Atomic, Molecular and Optical Physics
J. Phys. B: At. Mol. Opt. Phys. **52** (2019) 245401 (9pp) https://doi.org/10.1088/1361-6455/ab4cd9

Behavioral regimes and long-lived emitter states in mesolasers

Amine Abouzaid[1], **Walter Unglaub and A F J Levi**

Department of Electrical and Computer Engineering, University of Southern California, Los Angeles, CA 90089-2533, United States of America

E-mail: abouzaid@usc.edu

Received 3 May 2019, revised 23 September 2019
Accepted for publication 10 October 2019
Published 13 November 2019

Abstract

Emergence of long-lived emitter states is predicted to occur in a mesolaser driven below self-quenching threshold. Distinct behavioral regimes of the emitters are separated by peaks in photon fluctuations (the Fano factor) in a manner analogous to but fundamentally different from the nonequilibrium phase transition analogy in conventional lasers. The parameter space in which long-lived states emerge in mesolasers containing two or more emitters is identified and shown to be controlled by the strength of coupling to external baths.

Keywords: cavity quantum electrodynamics, microcavity lasers, quantum optics

(Some figures may appear in colour only in the online journal)

1. Introduction

As the number of emitters in a conventional macroscopic laser is reduced device behavior eventually enters a qualitatively different mesoscale regime dominated by quantum effects. Understanding and controlling the operation of mesoscale lasers consisting of several emitters (atoms or semiconductor quantum dots) in an optical cavity is currently a challenge that, if solved, can have practical ramifications [1–4]. For example, it may help lead the way to a new generation of efficient, ultra-small, lasers with important applications that include dense high-bandwidth optical interconnects in electronic systems.

The steady-state and transient average optical field intensity and average emitter excitation of a conventional *macroscopic* laser may be described using continuum mean-field rate equations. Such models are able to accurately predict important experimentally measurable quantities including laser threshold pump value, emitter excitation pinning above threshold, and critical slowing around threshold. Addition of Langevin noise terms to the model allows quantification of field and excitation fluctuations. The optical field of a macroscopic laser operating in the thermodynamic limit transitions from a disordered to an ordered state as the system is pumped from below to above lasing threshold. This is *the* classical example of a second-order non-equilibrium phase transition with the optical field as the order parameter [5–7]. However, apart from the presence of spontaneous emission, the continuum mean-field rate equations used to describe the behavior of a conventional macroscopic laser operating in the thermodynamic limit is classical. Recent research has focused on bridging the quantum-classical transition [8].

In dramatic contrast, a quantum mechanical description of a mesoscale laser admits the emergence of partially ordered *long-lived* emitter states for which there is no classical analog. In addition, no formal non-equilibrium phase transition exists in the finite-sized system. Instead, it is observed that the emergence and dissipation of the long-lived states creates behavioral regimes in the emitters that are identifiable in the photon statistics (the Fano factor) in a manner analogous to but different from the phases of conventional lasers. The presence of long-lived emitter states in mesoscale lasers is controlled by the strength of coupling to external baths and the number of emitters in the system. Physically, the stability of the long-lived states is a consequence of the phases carried by the emitters. For a state to be long-lived, these phases must cause destructive interference upon photon emission or absorption [9].

Emergence of long-lived two-emitter states in dissipative environments has been explored previously [10–14]. In the following, this behavior is analyzed in the context of mesolasers, and with reference to distinct behavioral regimes

[1] Author to whom any correspondence should be addressed.

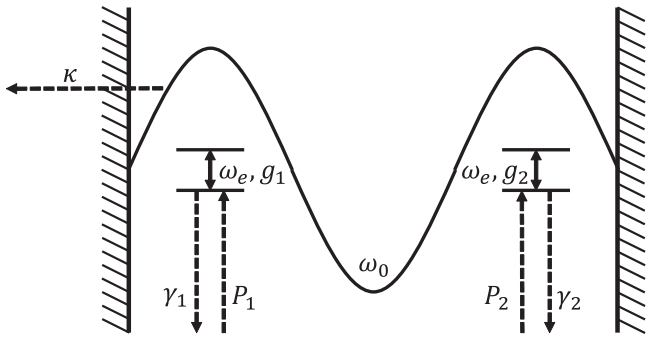

Figure 1. A schematic of the open-system model showing the case of two emitters, $N_e = 2$. The emitters are two-level systems with transition frequency ω_e. The pump terms P_1 and P_2 are the rate of transfer of excitations from the electron–hole reservoir to the first and second emitter, respectively. Similarly, γ_1 and γ_2 are the spontaneous emission rates into non-lasing modes, and g_1 and g_2 are the coupling rates to the cavity optical mode ω_0. The loss rate of the optical cavity mode into the environment due to finite mirror reflectivity is κ. The parallel mirrors of the Fabry–Perot cavity are shown on the left and right of the sketch.

associated with these states as a function of system parameters. Furthermore, it is shown that experimentally accessible parameters such as pump, mirror loss, and emission into non-lasing modes, may be used to change the fidelity of long-lived states in mesolasers containing two or more emitters.

2. Model

The system considered consists of a small number, N_e, of identical two-level emitters (atoms or semiconductor quantum dots) in a lossy Fabry–Perot optical cavity formed by two partially reflecting mirrors [15, 16]. The cavity contains a single optical mode that is on resonance with the emitters, so that the mode photon energy quantum $\hbar\omega_0$ is equal to the difference between the emitter energy levels $\hbar\omega_e$. A Jaynes–Cummings interaction models the coupling between the emitters and the optical mode [17, 18]. Emitters are excited by coupling to a pump reservoir of electron–hole pairs. Loss occurs due to leakage of photons from the optical cavity into the environment via transmission through the partially reflecting mirrors. There is also loss from emission into non-lasing modes. Figure 1 is a schematic illustration of the Fabry–Perot cavity for the particular case when the number of emitters is two, $N_e = 2$.

The sub-system of interest consists of N_e two-level emitters inside the optical cavity. Loss occurs due to interaction with the environment. For weak coupling the subsystem is the Jaynes–Cummings Hamiltonian in the rotating-wave approximation

$$H_{sub} = \hbar\omega_0\hat{b}^\dagger\hat{b} + \sum_{n=1}^{N_e}\hbar\omega_e\hat{\sigma}_n^\dagger\hat{\sigma}_n + \sum_{n=1}^{N_e}\hbar g_n(\hat{b}\hat{\sigma}_n^\dagger + \hat{b}^\dagger\hat{\sigma}_n), \quad (1)$$

where $\hat{\sigma}_n$ is the annihilation operator for the nth emitter, g_n is the coupling between the nth emitter and the photon field, and $\hat{b}$ is the annihilation operator that acts on a discrete positive integer number of photons occupying the optical cavity mode.

The interaction term for the pump reservoir is

$$\sum_{n=1}^{N_e}\sum_{R',R''}\mu_{R',R''}[\hat{d}_{R''}^\dagger\hat{c}_{R'}\hat{\sigma}_n^\dagger + \hat{d}_{R''}\hat{c}_{R'}^\dagger\hat{\sigma}_n], \quad (2)$$

where $\hat{c}_{R'}$ is the annihilation operator of electron–hole pairs in the reservoir, $\hat{d}_{R''}$ is the annihilation operator of phonons in the reservoir and $\mu_{R',R''}$ is the rate of transfer of excitations from the electron–hole pair reservoir to an emitter. Emission into non-lasing modes is described by the interaction term

$$\sum_{n=1}^{N_e}\sum_{R}\lambda_{lR}[\hat{\sigma}_n\hat{b}_R^\dagger + \hat{\sigma}_n^\dagger\hat{b}_R], \quad (3)$$

where $\hat{b}_R$ is the annihilation operator of photons in an external reservoir and λ_{lR} is the emission and absorption rate of photons in non-lasing modes. Transmission of photons in the cavity mode into the external photon reservoir is described by the term

$$\sum_{R}\lambda_R(\hat{b}\hat{b}_R^\dagger + \hat{b}^\dagger\hat{b}_R), \quad (4)$$

where λ_R is the rate of transfer of photons in a given mode between the cavity and the external reservoir.

The density matrix of the subsystem of interest may be calculated by tracing out the reservoir, so that

$$\hat{\rho} = \mathrm{Tr}(\hat{\rho}_T), \quad (5)$$

where $\hat{\rho}_T$ is the total system density matrix, including the reservoir, and the $\hat{\rho}$ is the density matrix of the subsystem of interest.

Assuming the external photon reservoir is at zero temperature, and disregarding pumping and spontaneous emission into non-lasing modes, the master equation for two-level emitters in a lossy optical cavity is [19]

$$\frac{d\hat{\rho}}{dt} = \frac{i}{\hbar}[\hat{\rho}, H_{sub}] + \frac{\kappa}{2}(2\hat{b}\hat{\rho}\hat{b}^\dagger - \hat{b}^\dagger\hat{b}\hat{\rho} - \hat{\rho}\hat{b}^\dagger\hat{b}). \quad (6)$$

By including additional analogous terms to account for pumping and spontaneous emission into non-lasing modes, the (Linblad) master equation for the cavity subsystem becomes [15, 16]

$$\begin{aligned}\frac{d\hat{\rho}}{dt} = &\frac{i}{\hbar}[\hat{\rho}, H_{sub}] + \frac{\kappa}{2}(2\hat{b}\hat{\rho}\hat{b}^\dagger - \hat{b}^\dagger\hat{b}\hat{\rho} - \hat{\rho}\hat{b}^\dagger\hat{b}) \\ &+ \sum_{n=1}^{N_e}\frac{\gamma_n}{2}(2\hat{\sigma}_n\hat{\rho}\hat{\sigma}_n{}^\dagger - \hat{\sigma}_n{}^\dagger\hat{\sigma}_n\hat{\rho} - \hat{\rho}\hat{\sigma}_n{}^\dagger\hat{\sigma}_n) \\ &+ \sum_{n=1}^{N_e}\frac{P_n}{2}(2\hat{\sigma}_n{}^\dagger\hat{\rho}\hat{\sigma}_n - \hat{\sigma}_n\hat{\sigma}_n{}^\dagger\hat{\rho} - \hat{\rho}\hat{\sigma}_n\hat{\sigma}_n{}^\dagger), \end{aligned} \quad (7)$$

where κ is the rate of optical loss from the cavity, γ_n is the rate of emission of the nth emitter into non-lasing modes, and P_n is the pump rate of the nth emitter via the introduction of excitations from an electron–hole reservoir. Note that because the pump term P_n can introduce excitations into the system, the electron–hole reservoir is not assumed to be at zero temperature. By letting $g_n = g\sin(\omega_0 x_n/c)$, where x_n is the position of the nth emitter in the cavity, the spatial

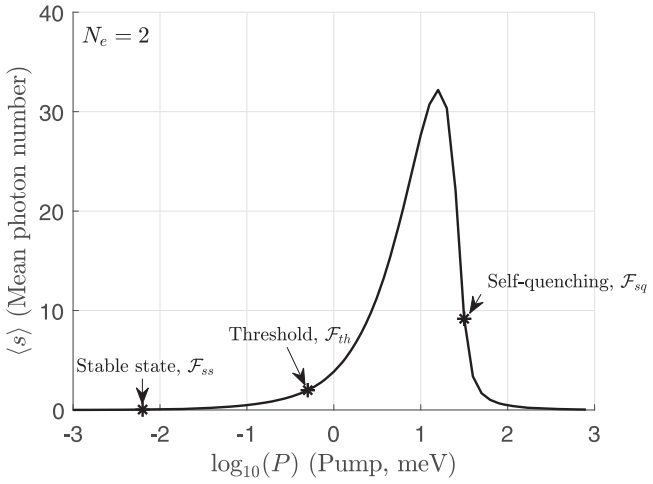

Figure 2. Mean photon number $\langle s \rangle$ as a function of pump for two emitters in a single-mode optical cavity with $g = 1$ meV, $\gamma = 10^{-3}$ meV and $\kappa = 0.25$ meV. The label $\mathcal{F}_{ss}$ indicates the value of $\langle s \rangle$ at which a local maximum in Fano factor occurs and is near the peak in fidelity of the long-lived (stable) state. $\mathcal{F}_{th}$ labels the value of $\langle s \rangle$ at which the Fano factor local maximum occurs corresponding to lasing threshold. $\mathcal{F}_{sq}$ indicates the value of $\langle s \rangle$ at which the Fano factor maximum occurs corresponding to self-quenching.

dependence of the atom-mode coupling may be taken into account. In the following, however, it has been assumed that the emitters are identical and are all located at positive anti-nodes of the cavity mode, so that $g_n = g$, $\gamma_n = \gamma$ and $P_n = P$.

The Lindbladian model disregards the time evolution of the environment. This means that any changes induced in the environment by the sub-system are not taken into account. It is implicitly assumed that the optical cavity is coupled to free space so that no photons that leave the optical cavity reenter.

3. State notation

The state of the system is determined by the presence of photons in the cavity (described by the density matrix $\hat{\rho}_p$) and the emitters (described by the density matrix $\hat{\rho}_e$). These are related to the density matrix of the system of interest (excluding the reservoir) $\hat{\rho}$ by the partial traces $\hat{\rho}_p = \mathrm{Tr}_e(\hat{\rho})$ and $\hat{\rho}_e = \mathrm{Tr}_p(\hat{\rho})$. Similarly, a pure product state of the total system can be written as $|\psi\rangle = |\psi\rangle_p \otimes |\psi\rangle_e$.

Since the cavity contains only a single mode, if s photons are in the cavity, then the photon state may be written as $|\psi\rangle_p = |s\rangle_p$. If it is known whether each of the N_e emitters is in the excited or ground state, then the emitter state may be written as $|\psi\rangle_e = |a_1 a_2 \ldots a_{N_e}\rangle_e$, where $a_n = 0$ if the nth emitter is in the ground state, and $a_n = 1$ if it is in the excited state.

The total state of a cavity with photon state $|s\rangle_p$ and with emitter state $|a_1 a_2 \ldots a_{N_e}\rangle_e$ is then

$$|\psi\rangle = |s\rangle_p |a_1 a_2 \ldots a_{N_e}\rangle_e = |s;\, a_1 a_2 \ldots a_{N_e}\rangle. \tag{8}$$

States of this form constitute a basis which may be used to express pure states.

For single excitation emitter states, the notation $|n\rangle_e = \hat{\sigma}_n |0\rangle_e$ is used to indicate the emitter state where the nth emitter is in the excited state, and the others are in the ground state.

4. Measures

4.1. Fidelity

Fidelity is used to evaluate the similarity of two density matrices. Given two matrices $\hat{\rho}_1$ and $\hat{\rho}_2$, the fidelity is

$$F(\hat{\rho}_1, \hat{\rho}_2) = \mathrm{Tr}[\sqrt{\sqrt{\hat{\rho}_1}\hat{\rho}_2\sqrt{\hat{\rho}_1}}\,]^2. \tag{9}$$

Its value is in the range [0, 1] and it takes on the value 1 if and only if $\hat{\rho}_1 = \hat{\rho}_2$. If $\hat{\rho}_1$ is a pure state, so that $\hat{\rho}_1 = |\phi_1\rangle\langle\phi_1|$, then the fidelity is

$$F(\phi_1, \hat{\rho}_2) = \langle\phi_1|\hat{\rho}_2|\phi_1\rangle. \tag{10}$$

4.2. Photon Fano factor

The Fano factor is used as a measure of spread in the photon number distribution, normalized to the mean photon number. It is defined as

$$\mathcal{F}(\hat{\rho}) = \frac{\sigma_s^2}{\langle s \rangle} = \frac{\mathrm{Tr}(\hat{\rho}\hat{s}^2) - \mathrm{Tr}(\hat{\rho}\hat{s})^2}{\mathrm{Tr}(\hat{\rho}\hat{s})}, \tag{11}$$

where the photon number operator $\hat{s} = \hat{b}^\dagger\hat{b}$ and $\langle s \rangle$ is the average number of photons in the optical cavity mode.

The Fano factor is related to the Mandel Q parameter by the relation

$$Q(\hat{\rho}) = \mathcal{F}(\hat{\rho}) - 1. \tag{12}$$

The Mandel Q parameter is a measure of the difference between a given distribution and the Poisson distribution.

5. Behavior of mesolasers

The steady-state behavior of mesolasers as a function of system parameters is the focus of the following discussion. Two separate numerical methods are used to produce and verify the results in this section [20]. First, time integration is used to generate the data shown in the figures. An optical cavity of the kind discussed in section 2 with $N_e = 2$ is initialized with no photons or excitations present. The cavity is then evolved in time using equation (7) and the fourth order Runge-Kutta method until the density matrix $\hat{\rho}$ reached steady state. To perform these calculations, the density matrix is truncated by choosing some maximum photon number that is much larger than the largest average photon number. These results are then verified by recasting equation (7) in the form

$$\frac{d\rho_{vect}}{dt} = \hat{\mathcal{L}}\rho_{vect}, \tag{13}$$

where ρ_{vect} is the vectorized density matrix and $\hat{\mathcal{L}}$ is the Linbladian superoperator. The steady-state solution is then

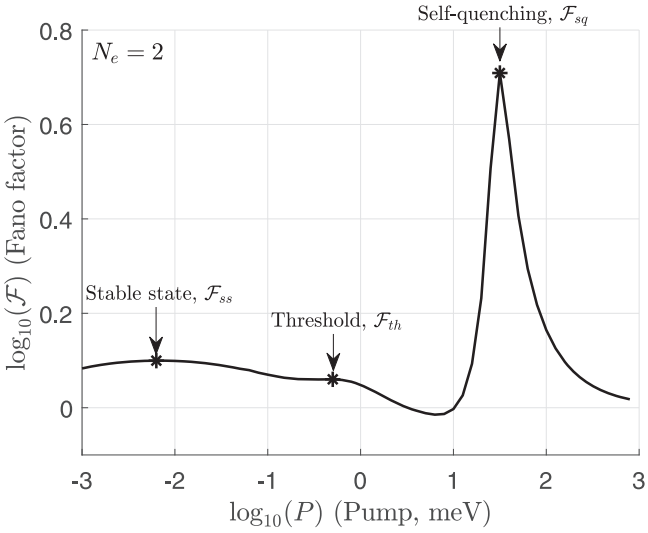

Figure 3. Photon Fano factor as a function of pump for two emitters in a single-mode optical cavity with $g = 1$ meV, $\gamma = 10^{-3}$ meV and $\kappa = 0.25$ meV. $\mathcal{F}_{ss}$ indicates the Fano factor local maximum at pump value $P_{ss} = P(\mathcal{F}_{ss})$ that occurs near the peak in fidelity of the long-lived (stable) state. $\mathcal{F}_{th}$ indicates the Fano factor local maximum corresponding to lasing threshold pump value $P_{th} = P(\mathcal{F}_{th})$. $\mathcal{F}_{sq}$ indicates the Fano factor maximum corresponding to self-quenching at pump value $P_{sq} = P(\mathcal{F}_{sq})$.

found by solving for the null space of the superoperator (i.e. setting $\frac{d\rho_{vect}}{dt} = 0$).

Figure 2 shows photon expectation value $\langle s \rangle$ as a function of pump for two emitters ($N_e = 2$) in a laser cavity with $g = 1$ meV, $\gamma = 10^{-3}$ meV and $\kappa = 0.25$ meV. With increasing pump, average photon number increases, peaks, and then decreases.

The value of pump at which photon number in the laser cavity rapidly increases is indicated by the local maximum in the Fano factor shown in figure 3 which, in this case, occurs at $\log_{10} P \approx -0.2$. The occurrence of Fano factor peaks at lasing threshold in conventional macroscopic lasers is established in the literature [21, 22]. The pump value $P_{th} = P(\mathcal{F}_{th})$ at which this Fano factor peak occurs is therefore defined as the lasing threshold in direct analogy with conventional macroscopic lasers while recognizing that, in fact, such a concept is only strictly valid in the thermodynamic limit.

The rapid decrease in photon number with increasing pump P corresponds approximately to the location of the peak in photon Fano factor $\mathcal{F}_{sq}$ at $\log_{10} P \approx 1.5$, indicating a transition to a new characteristic dynamic referred to as self-quenching. In this regime, high pump values prevent the emitters from de-exciting and emitting a photon. This has the effect of suppressing lasing while simultaneously increasing fluctuations, as expected by the fluctuation-dissipation theorem [23]. Previous work has established a connection between these fluctuations and Fano factor [24].

At values of $P < P_{th}$, a third peak in the Fano factor is easily identified and is associated with a transition to another behavioral regime (see $\mathcal{F}_{ss}$ in figure 3). This peak is not directly analogous to the known phase transitions in classical lasers and is best discussed in the context of a quantum stable state (see section 6.1). The peak in photon Fano factor, $\mathcal{F}_{ss}$, is not predicted by the classical continuum mean-field description because the cause is fundamentally quantum in origin.

6. Emitter states

In optical cavity systems of the type described above, there exist emitter states that do not interact with the optical cavity mode [9]. The emitter state of the system is defined as $\hat{\rho}_e = \mathrm{Tr}_p(\hat{\rho})$.

In particular, if the system contains two emitters ($N_e = 2$) with identical emitter-mode coupling rates $g_1 = g_2 = g$, then the anti-symmetric emitter Bell state

$$|\psi_-\rangle_e = \frac{1}{\sqrt{2}}(|10\rangle_e - |01\rangle_e) \tag{14}$$

cannot transition to any other state via emission or absorption of photons in the optical cavity mode [10]. This can be seen by calculating the transition energy $\langle\psi|\sum_{n=1}^{2} \hbar g(\hat{b}\hat{\sigma}_n^\dagger + \hat{b}^\dagger\hat{\sigma}_n)|\psi_-\rangle$ from $|\psi_-\rangle$ to any other state $|\psi\rangle$ mediated by the emitter-mode coupling term, where $|\psi_-\rangle = |s\rangle_p \otimes |\psi_-\rangle_e = \frac{1}{\sqrt{2}}(|s;\,10\rangle - |s;\,01\rangle)$ is the total system state with s photons and the anti-symmetric emitter state $|\psi_-\rangle_e$. Since

$$\sum_{n=1}^{2} \hbar g(\hat{b}\hat{\sigma}_n^\dagger + \hat{b}^\dagger\hat{\sigma}_n)\frac{1}{\sqrt{2}}(|s;\,10\rangle - |s;\,01\rangle) = 0 \tag{15}$$

it follows that no transitions to or from the state $|\psi_-\rangle_e$ are possible via interaction with the cavity mode.

More generally, consider single excitation emitter states of the form $|\psi\rangle_e = \sum_n a_n|n\rangle_e$, where $|n\rangle_e = \hat{\sigma}_n|0\rangle_e$. If $\sum_n a_n = 0$, then, as in the previous case, photon emission cannot occur (though absorption is possible for $N_e > 2$). Such states are longer-lived than other emitter states in optical cavities because one of the paths by which transitions between states occur is blocked.

Note that, unlike $|\psi_-\rangle_e$, the symmetric state

$$|\psi_+\rangle_e = \frac{1}{\sqrt{2}}(|10\rangle_e + |01\rangle_e) \tag{16}$$

is not stable. An optical cavity containing two ($N_e = 2$) identical emitters initialized with zero excitations present and allowed to evolve to steady state in the presence of a constant pump typically shows transient Rabi oscillations in fidelity for the symmetric $|\psi_+\rangle_e$ state. There are no such oscillations for the anti-symmetric state $|\psi_-\rangle_e$ since it does not interact with the optical cavity mode.

Naturally, an objective is to control the presence of these stable states in a meso-laser system by tuning system parameters such as P (the pump rate), γ (the emission rate into non-cavity modes) and κ (the optical loss rate).

6.1. Two emitter stable states

Figure 4 shows the fidelity $F(|\psi_-\rangle_e, \hat{\rho}_e)$ at steady state of the desired state $|\psi_-\rangle_e$ plotted as a function of pump, P. The fidelity versus pump in figure 4 is plotted for the indicated values of γ. Examination of the plot reveals that the optimal

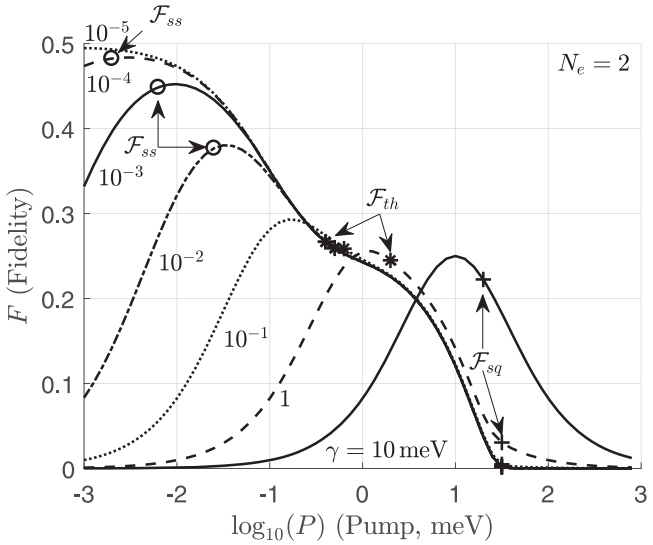

Figure 4. A semilogarithmic plot of fidelity ($F(|\psi_-\rangle_e, \hat{\rho}_e)$) as a function of pump (P) with $N_e = 2$. The different curves correspond to different values of γ, ranging from $\gamma = 10^{-5}$ meV to $\gamma = 10$ meV, and progressing by factors of 10. The lowest-fidelity curves on the left-hand side of the plot correspond to the highest values of γ. For all curves $g = 1$ meV and $\kappa = 0.25$ meV. The markers indicate the positions of Fano factor peaks on each fidelity curve. $\mathcal{F}_{th}$ and $\mathcal{F}_{sq}$ indicate Fano factor local maxima corresponding to lasing threshold and self-quenching, respectively. $\mathcal{F}_{ss}$ indicates Fano factor local maxima that occur near the peak fidelity of the stable emitter state $|\psi_-\rangle_e$.

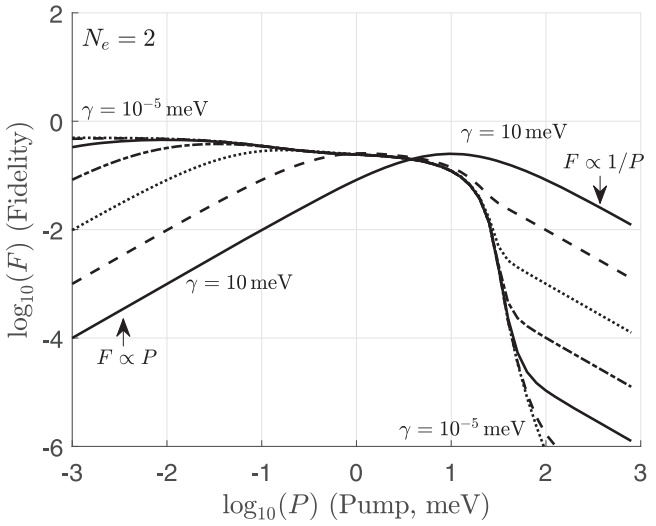

Figure 5. A log–log plot of fidelity ($F(|\psi_-\rangle_e, \hat{\rho}_e)$) as a function of pump (P) with $N_e = 2$. The different curves correspond to different values of γ, ranging from $\gamma = 10^{-5}$ meV to $\gamma = 10$ meV, and progressing by factors of 10. The lowest-fidelity curves on the left-hand side of the plot correspond to the highest values of γ. For all curves, $g = 1$ meV and $\kappa = 0.25$ meV.

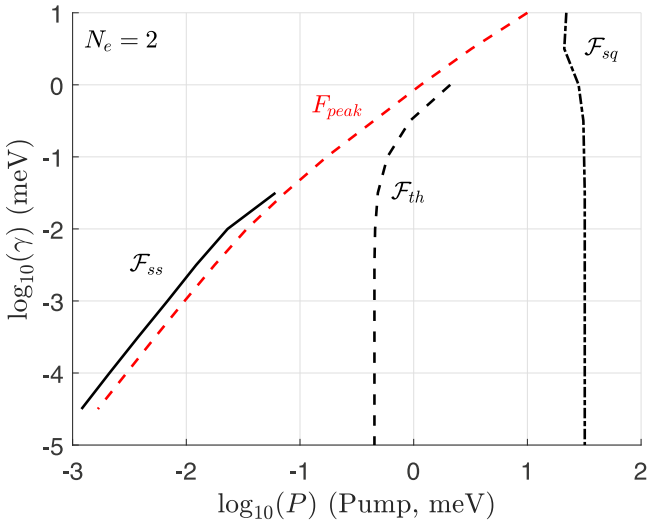

Figure 6. The black curves show values of pump, P, at which the Fano factor peaks for a given value of γ for $N_e = 2$ and $g = 1$ meV. Each of the three types of Fano factor peak, $\mathcal{F}_{ss}$, $\mathcal{F}_{th}$ and $\mathcal{F}_{sq}$, are plotted as separate curves. The red curve shows the location of the fidelity peaks F_{peak}. Spline fitting was used to accurately determine the locations of the peaks.

value of P is dependent on the value of γ. On the one hand, P contributes to the creation of states, and must be comparable to loss rates for any state to exist. On the other hand, P itself will cause the destruction of the desired state by introducing further excitations into it. Thus, fidelity peaks at pump value P_{peak}. The plot also reveals that lower values of γ allow higher fidelity to be achieved. This is consistent with the fact that γ directly disrupts the desired state. The maximum possible value of fidelity for $|\psi_-\rangle_e$ is 0.5 (see the appendix).

It is worth noting that, due to coupling to the environment, the system is in a mixed state once it reaches steady state. This is true of both the total state density matrix $\hat{\rho}$ and the emitter density matrix $\hat{\rho}_e$. For example, at $\kappa = 0.25$ meV, $\gamma = 10^{-5}$ meV and $P = 10^{-3}$ meV, we find that $\mathrm{Tr}(\hat{\rho}^2) \approx 0.49$ and $\mathrm{Tr}(\hat{\rho}_e^2) \approx 0.49$.

Figures 4 and 5 reveal that the four different behavioral regimes that the system may access are separated by local photon Fano factor maxima $\mathcal{F}_{ss}$, $\mathcal{F}_{th}$ and $\mathcal{F}_{sq}$. As best illustrated in figure 5, with increasing pump, P, first there is a linear increase in $F(|\psi_-\rangle_e, \hat{\rho}_e)$ until it approaches a peak. This initial linear increase is due to the fact that at low levels of excitation, it is far more likely that the pump will scatter the $|00\rangle_e$ state to $|\psi_-\rangle_e$ or $|\psi_+\rangle_e$ than that it will scatter the $|\psi_-\rangle_e$ or $|\psi_+\rangle_e$ states to the $|11\rangle_e$ state. Hence, to good approximation, all transitions will be from the $|00\rangle_e$ state to $|\psi_-\rangle_e$ or $|\psi_+\rangle_e$ (or conversely via spontaneous emission). Since the rate of these transitions is directly determined by the value of pump, the fidelity, which is a measure of the probability of occupation of these states, scales linearly with pump.

As pump increases further, fidelity gradually plateaus as transitions from $|\psi_-\rangle_e$ to $|11\rangle_e$ begin to counterbalance transitions from $|00\rangle_e$ to $|\psi_-\rangle_e$. At low values of γ, $P_{peak}^2 \propto \gamma$, where P_{peak} is the value of pump at which $F(|\psi_-\rangle_e, \hat{\rho}_e)$ peaks. This can be seen in figure 6, where the slope of the F_{peak} curve at low values of gamma is 2, indicating a quadratic relation between P_{peak} and γ. The parallel $\mathcal{F}_{ss}$ and F_{peak} curves at low γ in figure 6 suggest a link between the Fano factor peaks $\mathcal{F}_{ss}$ and peak fidelity F_{peak}.

Fidelity $F(|\psi_-\rangle_e, \hat{\rho}_e)$ then begins to decrease as higher pump increases the probability of occupation of the highest

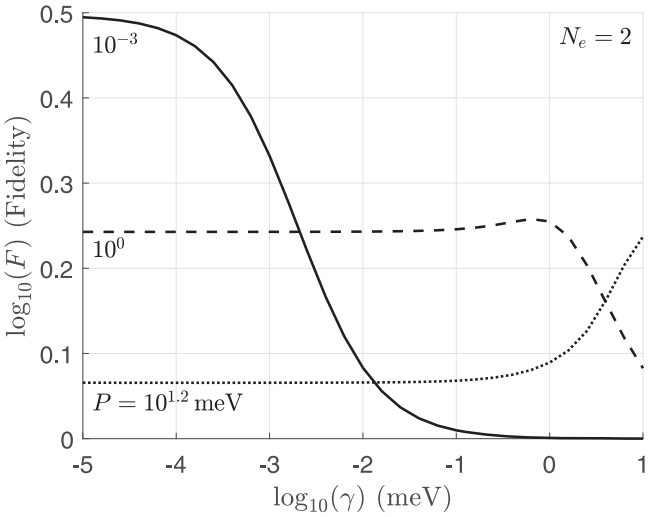

Figure 7. A semilogarithmic plot of fidelity ($F(|\psi_-\rangle_e, \hat{\rho}_e)$) as a function of spontaneous emission into non-lasing modes (γ) with $N_e = 2$. The different curves correspond to three different values of pump ($P = 10^{1.2}$ meV, $P = 10^{0}$ meV and $P = 10^{-3}$ meV). For all curves, $g = 1$ meV and $\kappa = 0.25$ meV.

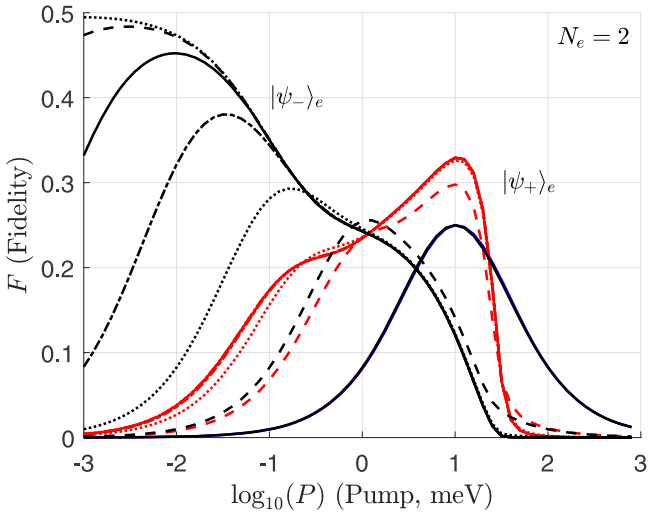

Figure 8. A semilogarithmic plot of fidelity as a function of pump with $N_e = 2$. The black curves show $F(|\psi_-\rangle_e, \hat{\rho}_e)$ while the red curves show $F(|\psi_+\rangle_e, \hat{\rho}_e)$. The different curves correspond to different values of γ, ranging from $\gamma = 10^{-5}$ meV to $\gamma = 10$ meV, and progressing by factors of 10. The lowest-fidelity curves on the left-hand side of the plot correspond to the highest values of γ. For all curves, $g = 1$ meV and $\kappa = 0.25$ meV.

energy state $|11\rangle_e$ while reducing the probability of occupation of the lowest energy state $|00\rangle_e$. A tipping point is reached beyond which the balance of transition rates between $|00\rangle_e$, $|\psi_-\rangle_e$ and $|11\rangle_e$ requires a decline in the probability of occupation of $|\psi_-\rangle_e$ (see figure A1 in the appendix for an illustration of these competing rates). The third regime involves a slowing of the decrease in fidelity as the system begins to lase. Pinning of fidelity and emitter-state occupancy due to lasing occurs over a finite range of pump, P. Finally, fidelity decreases as $1/P$ when the system experiences self-quenching and the emitters approach saturation (this occurs for all values of γ, though some of the curves have been truncated in figure 5).

At high values of γ, only the first (linear increase in fidelity) and fourth (inverse linear decrease in fidelity, self-quenching) regimes are present. The markers in figure 4 indicate where local maxima of the photon Fano factor occur. The locations of these maxima suggest the existence of three transitions between the four different behavioral regimes described above. At $\gamma \approx 0.1$ meV, the lower two Fano factor peaks merge, and only two peaks remain (lasing and self-quenching peaks). Nevertheless, the existence of the four behavioral regimes remains evident in the fidelity versus pump curves.

Photon statistics, in particular photon Fano factor, are convenient, experimentally measurable, quantities that may be used to distinguish between different behavioral regimes. Figure 6 plots the values of pump, P, at which Fano factor peaks for a given value of γ. The three types of Fano factor peaks, $\mathcal{F}_{ss}$, $\mathcal{F}_{th}$ and $\mathcal{F}_{sq}$, are indicated by three different curves which divide the parameter space into behavioral regions. Connections between curves are not shown because in these regions Fano factor peaks merge.

Figure 7 shows fidelity ($F(|\psi_-\rangle_e, \hat{\rho}_e)$) as a function of γ for three values of pump, P. It is notable that while for $P = 10^{-3}$ meV a significant difference in fidelity exists between high and low values of γ that would not be predicted by a semi-classical model, at high values of pump this contrast does not exist. Instead, the rise and fall in fidelity observed at high values of γ for $P = 10^{0}$ meV and $P = 10^{1.2}$ meV respectively is caused by the shifting of the location of the peak in fidelity due to higher pump values being required to achieve intermediate average excitation levels, while the constant value of fidelity at these values of pump for lower values of γ is caused by pinning due to lasing at $P = 10^{0}$ meV and by self-quenching at $P = 10^{1.2}$ meV.

Figure 8 compares $F(|\psi_-\rangle_e, \hat{\rho}_e)$ with $F(|\psi_+\rangle_e, \hat{\rho}_e)$. At low pump values, $|\psi_-\rangle_e$ dominates, as expected. Although the pump creates $|\psi_+\rangle_e$ and $|\psi_-\rangle_e$ with equal probability when occupation levels are low, as shown by the fact that for $\hat{\rho}_0 = |0;\,00\rangle\langle 0;\,00|$

$$\left.\frac{d\hat{\rho}}{dt}\right|_{t=0} = P(|0;\,10\rangle\langle 0;\,10| + |0;\,01\rangle\langle 0;\,01| - 2|0;\,00\rangle\langle 0;\,00|), \tag{17}$$

the fact that the symmetric state $|\psi_+\rangle_e$ interacts with the cavity optical mode while the anti-symmetric $|\psi_-\rangle_e$ does not implies that for low values of P and γ, $|\psi_+\rangle_e$ quickly dissipates into the environment via photon emission and photon transmission into the external photon reservoir (described by typically faster rates g and κ).

As pump increases, $F(|\psi_-\rangle_e, \hat{\rho}_e)$ peaks, and $F(|\psi_+\rangle_e, \hat{\rho}_e)$ begins to rise. This is because the higher pump values begin to disrupt $|\psi_-\rangle_e$, causing it to transition to the two-excitation state $|11\rangle_e$. The increased presence of this two-excitation state opens up a new pathway into $|\psi_+\rangle_e$ via photon emission. Once the lasing threshold is reached, there is a slowing in the rate of change of fidelity, as lasing stabilizes the emitter state via

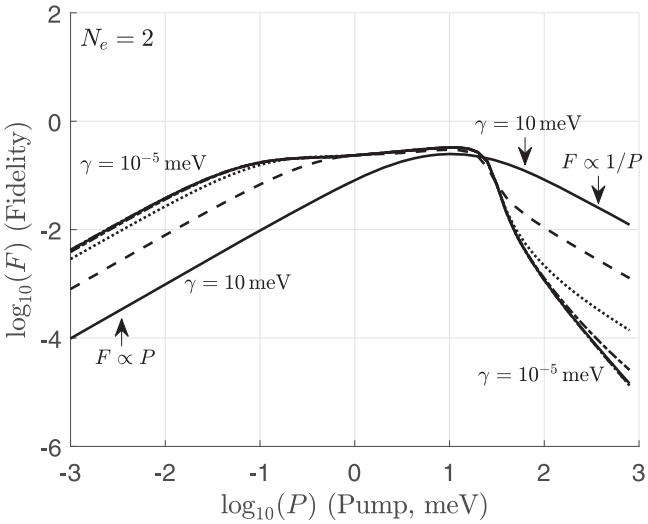

Figure 9. A log–log plot of fidelity ($F(|\psi_+\rangle_e, \hat{\rho}_e)$) as a function of pump (P) with $N_e = 2$. The different curves correspond to different values of γ, ranging from $\gamma = 10^{-5}$ meV to $\gamma = 10$ meV, and progressing by factors of 10. The lowest-fidelity curves on the left-hand side of the plot correspond to the highest values of γ. For all curves, $g = 1$ meV and $\kappa = 0.25$ meV.

pinning. Once quenching is reached, both single-excitation states disappear as the emitters approach saturation and the two-excitation state $|11\rangle_e$ dominates. For high values of γ, the fidelity curves for $|\psi_-\rangle$ and $|\psi_+\rangle$ become the same. This is because $\gamma \gg \kappa$ for large values of γ, so the distinction between $|\psi_+\rangle_e$ and $|\psi_-\rangle_e$ is negligible in this case.

Note that, as was previously observed for $|\psi_-\rangle_e$, and for the same reasons, $|\psi_+\rangle_e$ also initially undergoes a linear increase in fidelity at low values of pump, and a decrease in fidelity as $1/P$ at high values of pump. This can be seen in figure 9 which shows fidelity as a function of pump using a log–log plot.

At low values of P and γ, the steady-state fidelity decreases as κ decreases. This is because lower κ corresponds to a less lossy optical cavity in which more photons are stored. Hence, there is a higher probability of finding the system in the state $|\psi_+\rangle_e$ due to its interaction with the photon field, which means a lower probability of finding the system in the other states present at low values of P, namely $|00\rangle_e$ and $|\psi_-\rangle_e$.

When γ and P is small (e.g. $\gamma = P = 10^{-3}$ meV), the lifetimes of $|\psi_-\rangle_e$ and $|\psi_+\rangle_e$ may be approximated by identifying the fastest rate by which they scatter into other states. For $|\psi_+\rangle_e$, the fastest process is coupling to the cavity mode via $g = 1$ meV associated with the time constant $\tau_g \approx 1$ ps. On the other hand for $|\psi_-\rangle_e$, no interaction with the cavity mode occurs, so the fastest rates are P and γ. The lowest values of P and γ plotted in figure 8 are $\gamma = P = 10^{-3}$ meV with time constants $\tau_P = \tau_\gamma \approx 1$ ns. The difference between the lifetimes of $|\psi_-\rangle_e$ and $|\psi_+\rangle_e$ is therefore a factor of approximately 10^3. The consequence is a large difference in fidelity when comparing these states to the emitter density matrix. For example, if $\gamma = P = 10^{-3}$ meV, then $F(|\psi_-\rangle_e, \hat{\rho}_e)/F(|\psi_+\rangle_e, \hat{\rho}_e) \approx 120$.

6.2. Multi-emitter stable states

For three emitters ($N_e = 3$), two orthogonal stable states are:

$$|\psi_1\rangle_e = \frac{1}{\sqrt{3}}(|100\rangle_e + e^{i2\pi/3}|010\rangle_e + e^{i4\pi/3}|001\rangle_e), \quad (18)$$

$$|\psi_2\rangle_e = \frac{1}{\sqrt{3}}(|100\rangle_e + e^{i4\pi/3}|010\rangle_e + e^{i8\pi/3}|001\rangle_e) = \frac{1}{\sqrt{3}}(|100\rangle_e + e^{i4\pi/3}|010\rangle_e + e^{i2\pi/3}|001\rangle_e). \quad (19)$$

These are the only stable three-photon states, since the single-excitation space has dimension 3, and a third orthogonal state

$$|\psi_3\rangle_e = \frac{1}{\sqrt{3}}(|100\rangle_e + |010\rangle_e + |001\rangle_e) \quad (20)$$

is not stable.

For N_e emitters, there will always be $N_e - 1$ stable single-excitation states. This is because these states are the solutions to the equation $\sum_{n=1}^{N_e} a_n = 0$, which is a single equation in N_e variables, leaving $N_e - 1$ degrees of freedom. One basis for such states has the form

$$|\psi_j\rangle_e = \frac{1}{\sqrt{N_e}} \sum_{k=1}^{N_e} e^{2\pi ijk/N_e}|k\rangle_e \quad (21)$$

where $j = 1, 2, \ldots, N_e - 1$ [9]. The existence of $N_e - 1$ stable single-excitation states suggests that long-lived states can be present at low pump levels, even in macroscopic lasers. An accurate model describing scaling towards the thermodynamic limit in the number of emitters requires further research.

7. Conclusion

It has been shown that long-lived emitter states spontaneously emerge in mesolasers, and that they are associated with distinct behavioral regimes in different parts of the parameter space. Classical continuum mean-field models cannot predict the existence of these fundamentally quantum states.

When considered from the perspective of a quantum-classical transition, long-lived emitter-states are remarkably robust against coupling to the pump, P, emission into non-lasing modes, γ, and mirror loss, κ. For the two-emitter case ($N_e = 2$) with small γ, fidelity of the anti-symmetric state remains finite both below and above laser threshold and is only completely suppressed for pump values above self-quenching, $P > P(\mathcal{F}_{sq})$. For $P < P(\mathcal{F}_{sq})$ the long-lived anti-symmetric quantum state $|\psi_-\rangle_e$ only decoheres partially by coupling to a dissipative bath environment. Power law scaling of fidelity, F, with pump power, P, occurs as $F \propto P$ for $\gamma > P$ and as $F \propto 1/P$ for $P > P(\mathcal{F}_{sq})$.

Four distinct behavioral regimes are identified at different values of pump. These are associated with the emergence of the anti-symmetric emitter state ($P < P(\mathcal{F}_{ss})$), the dissipation of this state ($P(\mathcal{F}_{ss}) < P < P(\mathcal{F}_{th})$), lasing ($P(\mathcal{F}_{th}) < P < P(\mathcal{F}_{sq})$)

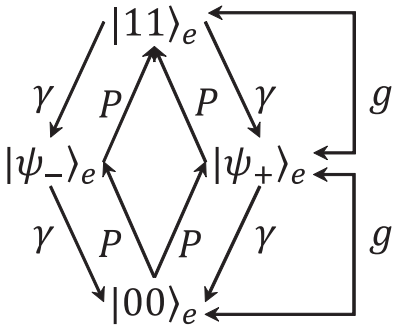

Figure A1. Schematic showing the four two-emitter ($N_e = 2$) states as well as the processes allowing for transitions between any two of the states. Pump (P) introduces an additional excitation, and therefore scatters $|00\rangle_e$ to $|\psi_-\rangle_e$ or $|\psi_+\rangle_e$ and scatters $|\psi_-\rangle_e$ and $|\psi_+\rangle_e$ to $|11\rangle_e$. Conversely, spontaneous emission into non-lasing modes (γ) removes excitations from the system, and therefore scatters $|11\rangle_e$ to $|\psi_-\rangle_e$ and $|\psi_+\rangle_e$, and scatters $|\psi_-\rangle_e$ and $|\psi_+\rangle_e$ to $|00\rangle_e$. Coupling between the cavity mode and emitters is represented by g, and allows for bi-directional transitions between $|\psi_+\rangle_e$ and $|00\rangle_e$ or $|11\rangle_e$. The anti-symmetric state $|\psi_-\rangle_e$ is isolated from the cavity mode.

and self-quenching ($P > P(\mathcal{F}_{sq})$). Future experimental measurement of photon Fano factor might be used to identify these four distinct behavioral regimes separated by local Fano factor peaks.

In general, the fidelity of long-lived states in mesolasers containing two or more emitters may be controlled by experimentally accessible parameters that include the number of emitters, pump, cavity mirror loss, and emission into non-lasing modes.

Appendix. Maximum fidelity

Figure 4 suggests that the maximum fidelity $F(|\psi_-\rangle_e, \hat{\rho}_e)$ that can be achieved in the two-emitter ($N_e = 2$) mesolaser is 0.5. This can be seen by observing that at low values of pump ($P = 10^{-3}$ meV) fidelity appears to approach 0.5 as γ approaches zero.

To show that this is the case, several approximations will need to be made. A convenient basis for the emitter states in a system with two two-level emitters consists of the four states $|00\rangle_e$, $|\psi_-\rangle_e$, $|\psi_+\rangle_e$ and $|11\rangle_e$. A schematic showing these four states, possible transitions between the states, and the processes enabling these transitions is shown in figure A1.

At low values of pump ($P \ll g$), photon expectation number $\langle s\rangle \approx 0$, so that the probability of photons being absorbed by the emitters is very small. Thus, at low levels of pump, only spontaneous emission into the cavity mode occurs primarily via g. Although Rabi oscillations between the emitters and a photon in the cavity mode may briefly occur, these oscillations will quickly dampen compared to most other timescales since $\kappa \gg P, \gamma$.

Because this spontaneous emission into the cavity mode occurs quickly with respect to other timescales, the probability of occupation of $|\psi_+\rangle_e$ and $|11\rangle_e$ is very low. These states become primarily occupied in transit as a path from

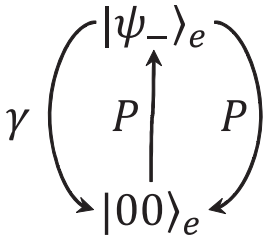

Figure A2. A simplified schematic showing the two dominant states at low values of P and γ. Pump (P) introduces excitations by scattering $|00\rangle_e$ to $|\psi_-\rangle_e$ or, indirectly via mostly unoccupied states and fast processes that have been omitted in this simplified schematic, removes excitations and scatters $|\psi_-\rangle_e$ to $|00\rangle_e$. Spontaneous emission into non-lasing modes (γ) removes excitations from the system and scatters $|\psi_-\rangle_e$ to $|00\rangle_e$. This introduces an asymmetry between the two states that becomes negligible if $\gamma \ll P$. See figure A1 for the full schematic.

$|\psi_-\rangle_e$ up to $|11\rangle_e$ via P and then quickly cascading back down to $|00\rangle_e$ through $|\psi_+\rangle_e$ via g. Because P is the slowest process in this path, it is the bottleneck. A simplified schematic can then be drawn as in figure A2. However, if $\gamma \ll P$, then γ can be ignored, and the system becomes symmetric. resulting in equal occupation of $|00\rangle_e$ and $|\psi_-\rangle_e$. This accounts for the maximum achievable fidelity of 0.5.

ORCID iDs

Amine Abouzaid https://orcid.org/0000-0002-9499-6894

References

[1] Nomura M, Kumagai N, Iwamoto S, Ota Y and Arakawa Y 2009 *Opt. Express* **17** 15975
[2] Atlasov K A, Calic M, Karlsson K F, Gallo P, Rudra A, Dwir B and Kapon E 2009 *Opt. Express* **17** 18178
[3] Jahnke F, Gies C, Assmann M, Bayer M, Leymann H A M, Foerster A, Wiersig J, Schneider C, Kamp M and Hofling S 2016 *Nat. Commun.* **7** 18178
[4] Wang T, Vergnet H, Puccioni G P and Lippi G L 2017 *Phys. Rev.* A **96** 013803
[5] DeGiorgio V and Scully M O 1970 *Phys. Rev.* A **2** 1170
[6] Graham R and Haken H 1970 *Z. Phys.* **237** 31
[7] Corti M and Degiorgio V 1976 *Phys. Rev. Lett.* **36** 1173
[8] Gartner P and Halati C M 2016 *Phys. Rev.* A **93** 013817
[9] Zanardi P 1997 *Phys. Rev.* A **56** 4445
[10] Beige A, Bose S, Braun D, Huelga S F, Knight P L, Plenio M B and Vedral V 2000 *J. Mod. Opt.* **47** 2583
[11] Braun D 2002 *Phys. Rev. Lett.* **89** 277901
[12] Benatti F, Floreanini R and Piani M 2003 *Phys. Rev. Lett.* **91** 070402
[13] Shao X Q, Wu J H and Yi X X 2017 *Phys. Rev.* A **95** 062339
[14] Chen X, Xie H, Lin G W, Shang X, Ye M Y and Lin X M 2017 *Phys. Rev.* A **96** 042308
[15] Perea J I, Porras D and Tejedor C 2004 *Phys. Rev.* B **70** 115304
[16] Roy-Choudhury K and Levi A F J 2011 *Phys. Rev.* A **83** 043827
[17] Jaynes E T and Cummings F W 1963 *Proc. IEEE* **51** 89

[18] Scully M O and Zubairy M S 1999 *Quantum Optics* (Cambridge: Cambridge University Press)
[19] Preskill J 1998 *Lecture Notes for Physics 229: Quantum Information and Computation* (Charleston, NC: CreateSpace Independent Publishing Platform)
[20] Navarrete-Benlloch C 2015 Open systems dynamics: Simulating master equations in the computer (arXiv:1504.05266v2)
[21] Rice P R and Carmichael H J 1994 *Phys. Rev.* A **50** 4318–29
[22] Jones B, Ghose S, Clemens J P, Rice P R and Pedrotti L M 1999 *Phys. Rev.* A **60** 3267–75
[23] Kubo R 1966 *Rep. Prog. Phys.* **29** 255
[24] Hiroshi H and Shimizu A 1997 *J. Phys. Soc. Japan* **66** 34–7